Influence of transition metal doping on the structural and optical properties of iron chromium nano oxides

M. Kalengay[1]*, T.N. Nsio[2], N.S.E. Osman[3]
[1]Department of Mathematics, Sciences and Sports Education, University of Namibia (Rundu)
[2]Department of Integrated Environmental Sciences, Faculty of Agriculture and Natural Resources, University of Namibia, Private Bag 5520 Oshakati, Namibia
[3]Institute of Laser, Sudan University of Science and Technology, P.O.Box 407, Khartoum 11113, Sudan

ARTICLE INFO

Article history:
Received: 7 June 2019
Received in revised form: 10 August 2019
Accepted: 13 August 2019
Published: 4 November 2019
Edited by DSI Iiyambo

Keywords:
Nanoparticles
Hydrothermal method
Structural properties
Optical properties

ABSTRACT

We have synthesized $Sn_{0.2}Fe_xCr_{1.8-x}O_3$ nano oxides with x$= 0.0, 0.1, 0.2, 0.3$. Single phase corundum structure and nanophase structure of the as-synthesized samples were confirmed by X-ray diffraction (XRD) and by transmission electron microscope (TEM). Crystallite sizes were calculated using the Scherrer's formula whilst particle sizes were obtained by TEM and found to be varying from 27.06 to 32.05 nm for the samples synthesized at different iron content. The optical measurements were performed by UV-visible spectroscopy. We observed that the band gaps and the refractive index vary with iron content.

1 Introduction

$Sn_{0.2}Fe_xCr_{1.8-x}O_3$ alloys are derived from the structure of hematite $\alpha-Fe_2O_3$ which has evidently attracted attention of chemists and physicists alike for many years [1]. Crystal structure is identical to corundum $\alpha-Al_2O_3$ with a closed-packed oxygen lattice and Fe^{3+} cations in octahedral sites. This alloy is anti ferromagnetic below the Morin transition of 250 K. It is in a weak ferromagnetic state after undergoing transition above the Morin temperature because of spin canting. It finally becomes paramagnetic at high temperatures of 948 K [2, 3]. The introduction of dopants modifies the optical and electronic properties of the alloy. The Fe^{3+} ions are substituted by Sn^{4+} ions in the corundum-related structure of $\alpha-Fe_2O_3$ with the formation of cationic and anionic vacancies [4, 5]. The difference in ionic radii between the two ions will influence the structural characteristics and phase behaviour of the doped system. The tin-doped $\alpha-Fe_2O_3$ alloys have been found to exhibit sensing properties for gases such as methane and carbon monoxide [6]. The performance of materials used as sensors and catalysts can be improved by reducing the particles sizes and increasing the surface area.

Photo-anodes for water splitting can be made from Hematite $\alpha-Fe_2O_3$ as it possesses several desirable properties [7]. The synthesis and characterisation of tin-doped iron oxides and tin-doped chromium oxides have been reported previously [8, 9]. Although there have been several studies of the $\alpha-Fe_{2-x}Cr_xO_3$ [10, 11], system, there appears to have been little activity in the optical and electronic properties of these materials. Therefore, in the present work, we report on the structural and optical properties of $Sn_{0.2}Fe_xCr_{1.8-x}O_3$ nano-crystals synthesized by hydrothermal method at different concentrations of Fe^{3+} and Cr^{3+}.

*Corresponding author: *E-mail address:* MKalengay@unam.na (M. Kalengay)

http://repository.unam.na/handle/11070/790 ISSN: 2026-7673; eISSN: 2026-8653/c 2019 ISTJN.

2 Materials and Methods

Nanocrystal $Sn_{0.2}Fe_xCr_{1.8-x}O_3$ alloys with x ranging from 0.0 to 0.3 were produced by the low temperature synthesis based on the hydrothermal process in a stirred pressure reactor (Parr 4843). The synthesis procedure is similar to what we have presented before [12] . Single-phase corundum compounds were prepared by mixing an aqueous solution of tin (II) chloride dehydrate with an aqueous solution of chromium (III) chloride hexahydrate and iron (III) chloride hexahydrate. Excess aqueous ammonia was added to the mixtures and the solutions boiled in a stirred pressure reactor for 3 hours. The resulting precipitate was filtered, washed with deionized water until no chloride ions were detected by the silver nitrate standard solution. The precipitate was washed with 95% ethanol and dried under an infrared lamp before calcinations in air at 600°C for 12 hours. The products were characterized by X-ray diffraction using a Phillips diffractometer with a cobalt source producing a beam of X-rays of radiation ($\lambda = 1.7903$Å).

A Jeol model JEM-1010 transmission electron microscopy (TEM) was used to obtain the particle sizes of the samples. Nano-material (powder) were prepared for spectrophotometric analysis using de-ionized water (H_2O) from UniLab SAARS6725000LL. Each substance was accurately weighted using an electronic balance. 50.0 mg of powder was diluted in 10 ml of solvent to make each sample. The UV-6300 PC Spectrophotometer (UQE1706002) with a wavelength range of 190 – 1100 nm at room temperature, was used to record the optical spectrum of the prepared sample. The UV-Vis Analyst-0001 software was used to display the spectrum.

3 Results and discussion

The XRD patterns of the as-prepared samples of $Sn_{0.2}Fe_xCr_{1.8-x}O_3$ with x$= 0.0, 0.1, 0.2, 0.3$ are shown in Figure 1.

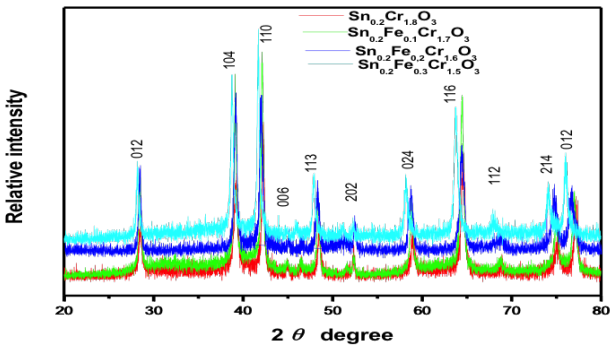

Figure 1: XRD patterns recorded for $Sn_{0.2}Fe_xCr_{1.8-x}O_3$ with x$= 0.0, 0.1, 0.2, 0.3$

All the patterns show single phase characteristic of corundum structures despite the presence of small impurities peaks. This has been previously observed for tin-doped $\alpha-FeCr_2O_3$ [9, 13]. Tin occupies similar sites in $\alpha-Fe_xCr_{1.8-x}O_3$ as it does in both $\alpha-Fe_2O_3$ and $\alpha-Cr_2O_3$ [12]. The average crystallite sizes (DXRD) were calculated using the Debye-Scherrer formula [14] while the particle sizes (DTEM) were obtained by transmission electron microscope (TEM). The TEM images in Figure 2 show that the particles are in nano-scale.

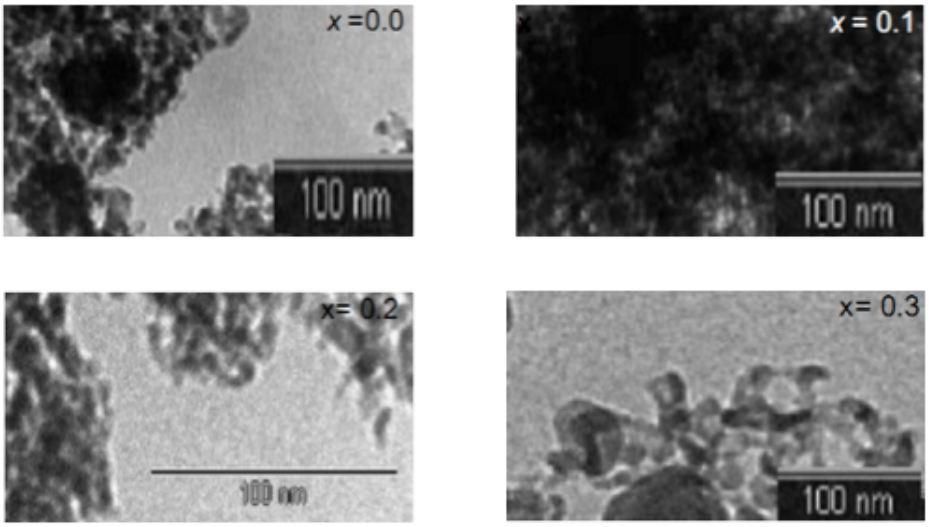

Figure 2: TEM micrographs for the as prepared $Sn_{0.2}Fe_xCr_{1.8-x}O_3$ samples with x$= 0.0, 0.1, 0.2, 0.3$

The values of $\mathrm{D_{XRD}}$ and $\mathrm{D_{TEM}}$ are recorded in Table 1. We observe that these values are almost identical. This can be due to the fact that the Scherrer equation is a rough approximation and it also depends on the number of the particles used to find the TEM values in this case (15). The values could be a little different if a Rietveld analysis was done. The crystallite sizes ($\mathrm{D_{XRD}}$) and particle sizes ($\mathrm{D_{TEM}}$) decrease as the iron content increases as shown in Figure 3.

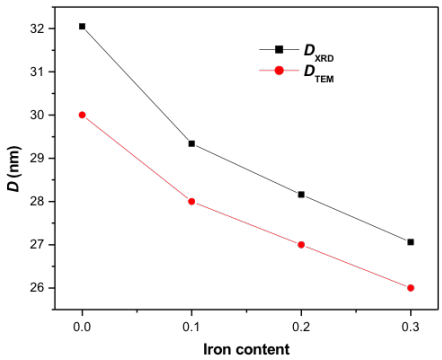

Figure 3: Variation of particle size with iron content for the as-prepared samples of $Sn_{0.2}Fe_xCr_{1.8-x}O_3$

The UV-Vis absorbance and transmittance spectra of the $Sn_{0.2}Fe_xCr_{1.8-x}O_3$ samples are shown in Figure 4 and Figure 5 respectively.

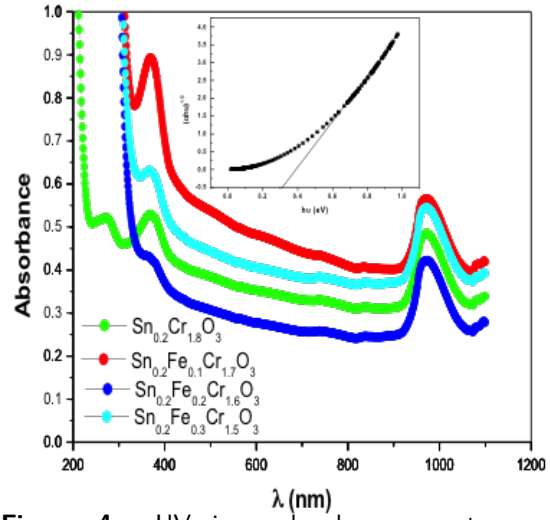

Figure 4: UV-vis. absorbance spectrum of $Sn_{0.2}Fe_xCr_{1.8-x}O_3$ nanoparticles.

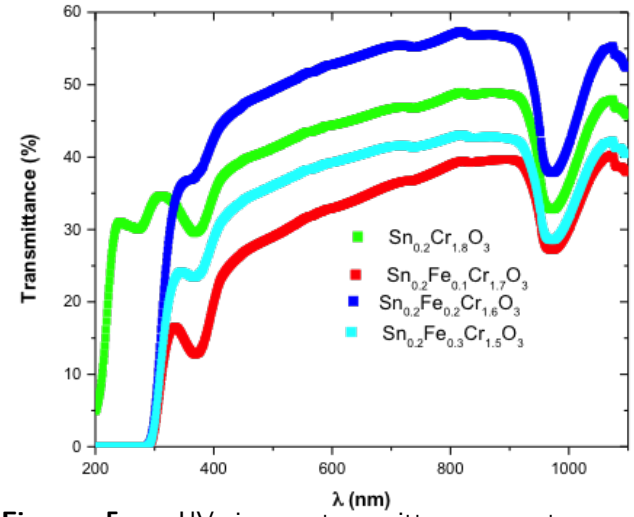

Figure 5: UV-vis. transmittance spectrum of $Sn_{0.2}Fe_xCr_{1.8-x}O_3$ nanoparticles.

The absorbance increases with iron content in the UV (200-400 nm) and decreases at around 390 nm where we observe a shift in absorbance edges before stabilizing in the visible range (400-800 nm). The average transmittance of the prepared samples increases from approximately 26% in the UV (200 - 400 nm) to 44% in the visible (400 - 800 nm) regions. The optical band gap energy (E_g) of the as-synthesized nano-particles is obtained from the UV-Vis spectra by using a well-known Tauc's relation [15]:

$$(\alpha hv) = A(hv - E_g)^n \tag{1}$$

where α is the absorption coefficient, A is a constant, E_g is the band gap energy of the material and exponent $n = \frac{1}{2}$ for direct transition. The value of the absorption coefficient can be determined by the following equation [16]:

$$\alpha = 2.303\left(\frac{\text{absorbance}}{t}\right), \tag{2}$$

where t is the thickness of the sample. The curves are plotted between $(\alpha hv)^{\frac{1}{2}}$ versus (hv) and extrapolation of the linear portions of the curves to the hv axis gives the energy gap as shown in the inset of Figure 4. The values of band gap are shown in Table 1. The optical band gaps calculated are found to be decreasing as the doping concentration of Fe increases and Cr decreases. The decrease in optical energy band gap could be due to the increase of density of localized state in the conduction band. The results show that the band gap energy E_g increases with decreasing particle size.

Table 1: Crystallite size ($\mathrm{D_{XRD}}$), particle size ($\mathrm{D_{TEM}}$), Energy band gap and refractive index for the as prepared $Sn_{0.2}Fe_xCr_{1.8-x}O_3$ samples.

x	$\mathrm{D_{XRD}}$ (nm) ± 0.4	$\mathrm{D_{TEM}}$ (nm) ± 2	Energy band gap (eV)	Refractive Index
0.0	32.05	30	0.08	7.5
0.1	29.34	28	0.13	6.6
0.2	28.16	27	0.38	4.5
0.3	27.06	26	0.48	4.3

This can be supported by the quantum confinement theory, which suggests that the holes in the valence band and the electrons in the conduction band are confined by the potential barriers of the surface. Because of the confinement of the electrons and holes, the band gap energy increases between the valence band and the conduction band with decreasing particle size [17]. We have also calculated the refractive index (n) of the as prepared samples of $Sn_{0.2}Fe_xCr_{1.8-x}O_3$ nano-particles using the following relation: $n = kE_g^C$; where $k = 3.3668$ and $C = -0.32234$. The refractive index shown in Table 1 increases as the energy band gap decreases as observed for different materials [18]. The refractive index is useful in determining the optical and electrical properties of the crystals. It can also be used in the design of heterostructure laser, in optoelectronic devices as well as in solar cell applications [19, 20, 21].

4 Conclusion

We synthesized the $Sn_{0.2}Fe_xCr_{1.8-x}O_3$ nano oxides with x$= 0.0, 0.1, 0.2, 0.3$ via hydrothermal methods in a pressure reactor and studied their structural and optical properties. XRD shows the corundum phase formation for all samples. TEM analysis shows that the average particle size of the samples decreases from 32.05 nm to 27.06 nm as the Fe concentration increases and the Cr concentration decreases. It is observed that the optical band gap decreases with increasing particle sizes while the refractive index increases.

Acknowledgements

We acknowledge the condensed matter group University of KwaZulu-Natal (UKZN) for measurements and the support from the University of Namibia (UNAM).

Abbreviations

NIST: National Institute of Standards and Technology 2, 3
SRM: Standard Reference Materials 2, 3
TEM: Transmission Electron Microscope passim
UV-Vis: Ultra-Violet and Vis

References

[1] L. Finger and R. Hazem, "Crystal structure and isothermal compression of Fe_2O_3, Cr_2O_3 and V_2O_3.," *Journal of Applied Physics*, vol. 51, pp. 5362–5367, 1980.

[2] W. F. Van Der, "Mossbauer effect in $\alpha-Fe_2O_3$," *Physica Status Solidi* (b), vol. 17, no. 1, p. 417–432, 1966.

[3] C. Shanshan, "Influence of Al substitution on magnetism and adsoption properties of hematite," *Journal Of Solid State Chemistry*, vol. 228, no. 2, pp. 82–89, 2015.

[4] C. A. Barrero, J. Arpe, E. E. Sileo, L. C. Sanchez, R. Zysler and C. Saragovi, "Ni-and Zn-doped hematite obtained by combustion of mixed metal oxinates," *Physica B: Condensed Matter*, vol. 354, no. 1, pp. 27 – 34, 2004.

[5] E. E. Sileo, D. Perez, A. Cesar, L. Larralde, S. Mariela and C. Saragovi, "Influence of the genesis on the structural and hyperfine properties of Cr-substituted hematites," *Chemical Geology*, vol. 238, no. 1 – 2, pp. 84 – 93, 2007.

[6] H. Kanai, H. Mizutani, T. Tanaka, T. Funabiki, S. Yoshida and M. Takano, "X-ray absorption study on the local structures of fine particles of $\alpha-Fe_2O_3$ -SnO_2 gas sensors," *Journal of Materials Chemistry*, vol. 2, no. 7, pp. 703–707, 1992.

[7] D. Christopher, K. Amit Agrawal, C. Erick Walter and D. Mark Vaudin, "Effect pf Tin doping on hematite photoanodes for water splitting," *Journal of Physical Chemistry C*, vol. 116, no. 29, pp. 15290 – 15296, 2012.

[8] F. J. Berry, O. Helgason, T. Moyo and X. Ren, "Tin doping of $\alpha-Cr_2O_3$ and $\alpha-(FeCr)_2O_3$," *Journal of Materials Sciences Letters*, vol. 59, no. 26, pp. 3241 – 3245, 2005.

[9] F. J. Berry, C. Greaves, O. Helgason, J. McManus, H. M. Palmer and T. R. Williams, "Structural and magnetic properties of Sn, Ti, and Mg-substituted $\alpha-Fe_2O_3$: A study by neutron diffraction and Mössbauer spectroscopy," *Journal of Solid State Chemistry*, vol. 151, no. 2, pp. 157 – 162, 2000.

[10] J. K. Srivastava, G. K. Shenoy and R. P. Shama, "Magnetic structure of Cr_2O_3 - Fe_2O_3 system," *Solid State Communications*, vol. 6, no. 2, p. 73–76, 1968.

[11] A. K. Bhattacharya, C. K. Majumdar, D. Chintalapudi and A. Hartridge, "A Mossbauer study of Fe_2O_3 - Cr_2O_3 nanocrystals dispersed in a silica matrix," *Journal of Magnetism and Magnetic Materials*, p. 183, 1998.

[12] K. Mbela, T. Moyo and J. Msomi, "Tin, manganese doped chromium iron oxides of composition $\alpha-Sn_{0.2}Cr_{1.8-x}Fe_xO_3$ and $Mn_{0.2}Cr_{1.8-x}Fe_xO_3$.," *Journal of Superconductivity and Novel Magnetism*, vol. 25, pp. 2637–2641, 2012.

[13] I. Ayub, C. Johnson, D. A. Johnson, E. A. Moore, X. Ren and H. M. Widatallah, "Tin-, titanium-, and magnesium-doped $\alpha-Cr_2O_3$: characterisation and rationalisation of the structures," *Solid State Communications*, vol. 123, no. 3 - 4, pp. 141 – 145, 2002.

[14] X. Qi and D. Wu, *J. Magn. Magn. Mater*, vol. 666, p. 320, 2008.

[15] J. Tauc, Amorphous and liquid semiconductors, New York: Plenum, 1974.

[16] J. W. Robinson, Atomic Spectroscopy, 2nd Edition ed., New York: Taylor & Francis, 1996.

[17] M. Singh, M. Goyal and K. Devlal, "Size and shape effects on the band gap of semiconductor compound nanomaterials," *Journal of Taibah for University of Science*, vol. 12, no. 4, pp. 470–475, 2018.

[18] V. Kumar and J. Singh, "Model for calculating the refractive index of different materials," *Indian Journal of Pure & Applied Chemistry*, vol. 48, pp. 571–574, 2009.

[19] Y. Akaltum, M. Yildirim and A. Ates, "The relationship between refractive index-energy gap and the film thickness effect on the characteristic parameters of CdSe thin films," *Optics Communications*, vol. 284, no. 9, pp. 2303-2311, 2011.

[20] N. Bouarissa, "Pseudopotential calculations of $Cd_{1-x}Zn_xTe$: Energy gaps and dielectric constants," *Physica B*, vol. 399, no. 2, pp. 126–131, 2007.

[21] F. Mezrag, W. K. Mohamed and N. Bouarissa, *Physica B*, vol. 405, pp. 2272–2276, 2010.